A COMBINED GEOMETRIC APPROACH FOR COMPUTATIONAL FLUID DYNAMICS ON DYNAMIC GRIDS

John W. Slater [1]
NASA Lewis Research Center
Cleveland, Ohio 44135

SUMMARY

A combined geometric approach for computational fluid dynamics is presented for the analysis of unsteady flow about mechanisms in which its components are in moderate relative motion. For a CFD analysis, the total dynamics problem involves the dynamics of the aspects of geometry modeling, grid generation, and flow modeling. The interrelationships between these three aspects allow for a more natural formulation of the problem and the sharing of information which can be advantageous to the computation of the dynamics. The approach is applied to planar geometries with the use of an efficient multi-block, structured grid generation method to compute unsteady, two-dimensional and axisymmetric flow. The applications presented include the computation of the unsteady, inviscid flow about a hinged-flap with flap deflections and a high-speed inlet with centerbody motion as part of the unstart / restart operation.

INTRODUCTION

The computation of the unsteady fluid dynamics about mechanisms with components in relative motion has become an important topic in computational fluid dynamics (CFD) [1-5]. One example of such a mechanism is the NASA Variable Diameter Centerbody (VDC) inlet in which the axisymmetric centerbody can translate and change diameter to adjust the mass flow rate and stabilize the flow [6,7].

The CFD analysis process involves the aspects of geometry modeling, grid generation, and flow modeling, as shown in figure 1. When the components of the mechanism are not in relative motion, the geometry model, if one exists, is used to generate a grid, which is then used in the flow model and computation. The flow may, or may not, be a function of time. If no solution adaptive grid method is used, the grid remains fixed for the time interval of the analysis. This process is sequential with information being passed in one direction from the geometry model to the grid to the flow model.

When the components of the mechanisms are in relative motion, the geometry modeling, grid generation, and flow modeling all become a function of time. The main flow of information continues to be from the geometry model to the grid to the flow model. However, the geometry modeling and grid generation take on an increased importance. The interrelationships between the geometry modeling, grid generation, and flow modeling become more important and are discussed. The approach presented here attempts to use these interrelationships advantageously to enhance the overall computation of the total dynamics problem.

The focus of the approach is placed on the establishment of a geometry model, which is composed of a collection of geometric entities representing the components of the mechanism. This allows for accurate modeling of the mechanism and specification of the geometry motion. The existence of a geometry model allows the possibility for transfer of geometry data in the

[1]National Research Council Associate, CFD Branch, Internal Fluid Mechanics Division

form of standardized computer-aided-design (CAD) file formats such as the NASA-IGES format [8]. The work here considers planar geometry with the motion of a geometric entity assumed to be a rigid body motion.

The flow domain is the enclosed control volume in which the flow equations are solved. The modeling of the boundary of the domain is generally considered part of the geometry modeling because the domain boundary entities usually have the same mathematical form as the geometric entities. The approach presented here places a greater distinction between the geometric entities and the domain boundary entities because of the possibility of the relative motion of the geometric entities.

When there is relative motion of the components of the mechanism, it is possible that the grid will be regenerated in some manner at each time step of the computation. This requires an efficient grid generation approach. A multi-block, structured grid topology is used in the work presented here. This choice of topology is due to the desire for accurate and efficient computation of unsteady, viscous flows. It is assumed that the block topology remains fixed during the time interval of the computation. This restricts the extent of the geometry motion to moderate levels. The approach presented here involves the full use of the geometry and flow models in the grid generation. The grid generation information is associated with the geometric and domain boundary entities to ensure accurate generation of the boundary grid and grid dynamics. The association provides a natural formulation of the grid generation problem, which is used to implement some automation into the grid generation problem. An algebraic, sub-block method is used to efficiently generate the grid while providing for high grid quality. The same approach is used to compute the grid dynamics.

A mixed Eulerian-Lagrangian description of the integral form of the Navier-Stokes equations accounts for the motion of the geometry and flow domain. These equations are discretized for a cell-vertex, finite-volume approximation. The motion of the cell-faces of the finite-volume are based on the grid speeds. A time-accurate method is used to integrate the finite-volume equations. The approach presented here associates the flow boundary conditions with the geometric and domain boundary entities; allowing a natural specification of the boundary conditions and improving the association of the flow with the geometry model and grid.

The approach introduced above attempts to use the interrelationships between the aspects of geometry modeling, grid generation, and flow modeling for the full benefit of the computation of the total dynamics problem. Because of these interrelationships and the focus on the geometry modeling, the approach is referred to as the *combined geometric approach for CFD.*

The details of the approach are presented in the following sections. Some applications of the approach are presented in the analysis of a hinged flap with sinusoidal flap motion and the VDC inlet during the unstart / restart operation involving the motion of the centerbody.

GEOMETRY MODELING

A mechanism is assumed to consist of a set of components defined by some assembly information. The components may move relative to each other according to some kinematic relation as a function of time. The configuration of the mechanism is the spatial relationship of the components at a certain time. The work presented here assumes that each component moves as a rigid body in translation and rotation about a point; and not as a deformable body.

A mechanism used to illustrate the concepts of the approach is the NASA Variable Diameter Centerbody (VDC) inlet [6,7]. The VDC inlet is a mixed-compression inlet being studied at the NASA Lewis Research Center as a concept for a high-speed inlet for transport aircraft. Figure

2 shows the mechanical design of the VDC inlet. The VDC inlet is designed to operate at a cruise Mach number of 2.5 with a 45% internal contraction of the flow using a biconic forward centerbody. The second and aft cones of the centerbody consist of overlapping leaves which form an umbrella mechanism which allows the diameter of the centerbody to change to vary the mass flow of air into the inlet. The centerbody may also translate to adjust the mass flow rate. There is a bleed slot in the centerbody and bleed holes on the forward interior of the cowl for the stabilization of the normal shock and improvement of the pressure recovery.

The geometry model of the mechanism consists of a collection of geometric entities which model the individual components. The geometric entities are defined numerically using a parametric coordinate related to the arclength along the entity. The methods of computer-aided-design (CAD) provide standard procedures for generating such models as mathematical curves and surfaces [9]. An effective numerical representation of the geometry is the non-uniform rational B-spline (NURBS) representation. The NASA-IGES format [8], a subset of the Initial Graphics Exchange Standard (IGES), provides a standard format for transfer of geometry data. In a design environment, one might expect a geometry model would already exist as part of the CAD effort and would be available for the CFD analysis.

The work presented here considers a planar geometry model as would be needed for a two-dimensional or axisymmetric CFD analysis. Each component of the mechanism is modeled as a single geometric entity (m), represented either as a line segment or a cubic spline curve using the parametric coordinate (u), which corresponds to the arclength along the geometric entity. Figure 3 shows the planar geometry model for the VDC inlet with the individual geometric entities identified.

Each geometric entity is assumed to move as a rigid body, which allows an efficient modeling of the geometry using the parametric coordinate since the mathematical description of the curves only needs to be computed once, at the start of the computation.

The variable centerbody of the VDC inlet is modeled by specifying the dynamics of certain entities. The change in diameter of the centerbody is modeled by the rotation of the geometric entities defining the second and aft cones about their respective points of rotation as shown in figure 3. The translation of the centerbody is modeled by the translation of the geometric entities defining the centerbody nose, second cone, aft cone, and aft centerbody. The dynamics of these geometric entities are defined by simple kinematic relations. Figure 4 shows a variation of the centerbody in which the centerbody has translated forward and the second-cone has rotated to match the angle of the nose cone.

Geometric information is obtained from the geometry model as a function of the geometric entity (m), parametric coordinate (u), and time (t). Information that is available is the position coordinates ($\vec{r}$), velocity ($\dot{\vec{r}}$), tangent vector ($\hat{t}$), normal vector ($\hat{n}$), acceleration ($\ddot{\vec{r}}$), second-derivative ($\vec{r}\,''$), and curvature (κ). A single subroutine in the code provides this information by referencing the geometry model and entity kinematic state for the given time.

This approach for the geometry modeling may seem excessive for a simple planar geometry, but it sets a framework for the handling a more complex geometry model for three-dimensional mechanisms.

DOMAIN MODELING

The domain modeling involves defining the boundary of the flow domain. Part of the boundary will consist of the geometric entities of the geometry model. The remaining part of the boundary requires domain boundary entities to be defined such that the flow domain is enclosed.

The domain boundary entities are defined mathematically the same as the geometric entities of the geometry model. Thus, the domain boundary entities may be specified in the same manner as the geometry model. In figure 3, the domain boundary entities include the inflow, farfield, and outflow entities.

The relative motion of some of the geometric entities of the geometry model requires that some domain boundary entities be of variable geometric representation. These entities are called variable domain boundary entities. For the planar VDC inlet model shown in figure 3, the bleed slot entity will be of variable shape as the second cone and aft cone are rotated. As the centerbody is translated, the axis-of-symmetry and aft centerbody entities will change shape. Figure 4 shows the change of shape in these variable domain boundary entities.

Defining the flow domain is a secondary task in the CFD analysis and one suited for automation. Such automation will require the use of information about the geometry and flow models. The approach presented here provides a framework for providing that information.

GRID GENERATION

When there is relative motion of the geometric entities, the grid becomes a function of time. The grid will then be regenerated in some manner for each time step in the CFD analysis. This requires an efficient grid generation method.

The work presented here uses a multi-block, structured grid topology with grid lines matching contiguously across blocks. The choice of this topology was due to the desire for accurate and efficient computation of viscous flows. Further, the problems of interest (VDC inlet) did not warrant a more general grid topology such as overset or unstructured grids. Yet, many of the ideas of the approach are applicable to other grid topologies.

For the planar domains of this work, a block is a quadrilateral. A face of the quadrilateral is defined by specifying the entities which comprise the face. To enclose the quadrilateral, block interface entities may have to be defined. The block interface entities also divide two blocks in the domain. These are represented in the same mathematical form as the geometric and domain boundary entities. Thus the block interface entities may be specified in the same manner as the geometry model. Figure 3 shows the block interface entity for the VDC inlet.

The block represents a (ξ, η) generalized coordinate system. The generalized ξ-coordinate of the structured block is commonly directed in the streamwise direction while the generalized η-coordinate is commonly directed in the transverse flow direction. To reduce the amount of work required to generate a grid, each block is limited to only one entity in the η-direction (ξ_{min} and ξ_{max} faces).

It is assumed that the topology of the block remains fixed throughout the computation. This imposes a limitation on extent of the motion of the components and limits the generality of the approach, but it minimizes the amount of work required to regenerate the grid at each times step.

The grid generation is performed efficiently by the use of algebraic methods. Quality grids are obtained by sub-dividing a block into sub-blocks according to the geometric features of the entities. Each sub-block is usually small enough to approximate the shape of a generalized "rectangle". A face of a sub-block contains at most one entity and may contain only a portion of an entity.

Figure 5 shows how the domain for the VDC inlet has been divided into two blocks with sub-blocks. The first block extends from the inflow boundary through the diffuser to the compressor face. Block 2 extends from the inflow boundary over the cowl to the exterior outflow boundary.

Since there is only one entity along in the η-direction of a block, the entities that define the η-constant boundaries of each sub-block are defined. The ξ-constant boundaries of the sub-block are either the ξ_{min} boundary of the block, the ξ_{max} boundary of the block, or a sub-block boundary. The sub-block boundary is defined using a two-point cubic spline with the endpoint tangents specified as the normal vectors of the entities on the η_{min} and η_{max} faces of the sub-block. Figure 5 shows how these sub-block boundary curves intersect the entities at right angles. This orthogonality helps generate an interior grid that is orthogonal to the entities.

The endpoint normal vector used to construct the sub-block boundary curve may have different directions if the slopes of the entities at a junction of two entities do not match. This is illustrated in figure 6. The choice of which normal vector to use is based on the flow boundary conditions for the entities. For example, if entity B is a solid wall boundary condition while entity A is a freestream boundary condition, the normal vector from entity B would be used since it is felt that it is more important to resolve the solid wall flow than the freestream flow.

One feature of the combined geometric approach is that the grid generation information such as grid density, grid spacing along the boundary, and grid spacing normal to the boundary is associated with the geometric entities. This allows for a more natural procedure for the specification of this information. One can sense the number of grid points and the spacings that may be needed to resolve the flow along and normal to an entity. One constraint is that the number of grid points need to match across the block and not introduced excessive grid line skewing.

Once, the geometry of the sub-block is defined, the grid density and spacing are defined along the boundaries. A hyperbolic tangent method is generally used to distribute the boundary grid points with respect to the parametric coordinate of the geometric entity [10]. Each boundary grid point is associated with a parametric coordinate on a geometric entity. This ensures that the boundary grid will always adhere to the time-dependent geometry.

The association of the grid and geometry allow geometric information such as position coordinates ($\vec{r}$), velocity ($\dot{\vec{r}}$), tangent vector ($\hat{t}$), normal vector ($\hat{n}$), acceleration ($\ddot{\vec{r}}$), second-derivative ($\vec{r}\,''$), and curvature (κ) to be available for use in the grid generation methods.

In a CFD analysis, grid generation is a secondary activity in that it is a means to an end: the computation of the flowfield. Ideally, grid generation should be fairly automatic and transparent to the analyst. Proper automation of grid generation requires information on the geometry and flow conditions. The interrelationships between the geometry model, grid, and flow model as highlighted in this approach lends itself to an automated procedure for determining the grid density and spacing along the entities. Using information on the geometric properties of the entity, the flow boundary conditions, and grid quality parameters such as minimum and maximum grid spacing, maximum grid spacing ratio, and minimum and maximum grid aspect ratio, the appropriate number of grid points and their spacing are determined along each entity.

Once the grid points are distributed along the sub-block boundaries, the volume grid can be generated using a transfinite-interpolation method. Since a sub-block maintains a fairly "rectangular" shape, a transfinite-interpolation works well.

Figure 7, 8, 9 show examples of grid generated using the sub-block, algebraic grid method. The grid for the VDC inlet is shown for the entire domain in figure 7, while figure 8 shows a close-up of the grid in the throat region of the VDC inlet with the centerbody moved. Figure 9 shows the grid for the hinged-flap at a 15 degree angle-of-attack.

The motion of the geometry requires the grid motion to be computed for each time step. Several strategies are investigated for generating the dynamic grid and computing the grid speeds. First, one can regenerate the grid at each point in time based on the current configuration

of the geometric model. The grid speeds can then be determined through a time-difference of a sequence of grids. A second strategy is to start with an initial grid and deform it as a geometric entity is moved. Again the grid speeds can be determined through a time-difference. A third strategy is to start with an initial grid and directly compute the grid speeds as a boundary-value-problem using the knowledge of the velocities of the entities. The time-dependent grid is then obtained through a time-integration of the grid speeds.

FLOW MODELING

The integral form of the Navier-Stokes equations for a time-varying control volume is

$$\frac{d}{dt}\int_{V(t)} U\, dV + \oint_{S(t)} \mathbf{H}\cdot\hat{n}dS = 0 \tag{1}$$

where U is the algebraic vector of conservative variables,

$$U^T = \left(\rho,\ \rho\vec{V},\ E_t\right) \tag{2}$$

where for a perfect gas,

$$E_t = \rho\left[e + \frac{1}{2}\left(\vec{V}\cdot\vec{V}\right)\right]$$

and p and ρ are the primitive variables of pressure, and density. The velocity vector, $\vec{V}$, in Cartesian coordinates is

$$\vec{V} = u\,\hat{\imath} + v\,\hat{\jmath}. \tag{3}$$

The $\mathbf{H}$ is the flux dyadic, which for a mixed Lagrangian-Eulerian description [11] is,

$$\mathbf{H} = \mathbf{F} - \vec{g}\,U. \tag{4}$$

The $\vec{g}$ is the velocity vector of the boundary of the control volume. In Cartesian coordinates, it is

$$\vec{g} = x_\tau\,\hat{\imath} + y_\tau\,\hat{\jmath}. \tag{5}$$

An Eulerian description is obtained for $\vec{g} = 0$ while a Langrangian description is obtained for $\vec{g} = \vec{V}$.

The $\mathbf{F}$ is the Cartesian flux dyadic for the two-dimensional, unsteady Navier-Stokes equations. The flow equations are complete with Sutherland's formula, the definition of the Prandtl number, and the assumptions of a perfect gas (air) and laminar viscous flow. A Reynolds averaging is used to approximate turbulence effects and a turbulence model provides the eddy viscosity.

The flux dyadic can also be expressed as

$$\mathbf{H} = \mathbf{C} - \mathbf{D}, \tag{6}$$

where $\mathbf{C}$ is the portion of the flux dyadic containing the convective terms,

$$\mathbf{C} = \left(\vec{V} - \vec{g}\right)U, \tag{7}$$

and $\mathbf{D}$ is the portion of the flux dyadic containing the non-convective terms.

Equation 1 can be expressed in a compact form of

$$\frac{d\hat{U}}{dt} + \hat{R} = 0 \tag{8}$$

where

$$\hat{U} = \int_{V(t)} U \, dV \tag{9}$$

and

$$\hat{R} = \oint_{S(t)} \mathbf{H} \cdot \hat{n} dS. \tag{10}$$

The solution of the flow equations require the specification of the flow boundary conditions. One feature of the combined geometric approach is that the boundary conditions are associated with the entities of the geometry model. For example the curves defining the surfaces of the inlet (i.e. nose cone, cowl, etc...) are specified to be solid wall boundary conditions which are slip surfaces for inviscid flow analysis and non-slip walls for viscous flow analysis. The flow domain boundaries not representing the inlet surfaces are specified to be inflow or outflow boundaries. Associating the flow boundary conditions with entities allows the possibility that for a moving geometry and grid, the boundary grid points move from one geometric entity to another. Thus, the grid point may change the type of boundary condition with which it is associated.

One issue that arises is what boundary condition to impose at a grid point located at the junction of two entities if the entities are associated with different boundary condition types? These issues are resolved by defining a hierarchy for the flow boundary conditions. For example, at the junction of an entity defined as a non-slip wall and an entity defined as an inflow boundary, the non-slip wall would get more priority and the boundary grid point would be imposed as a non-slip boundary condition.

The existence of a geometry model allows its use by the flow boundary condition modeling. The physical boundary condition for a slip wall can be specified as

$$\rho_B \left(\vec{V}_B - \vec{g}_B \right) \cdot \hat{n} = \dot{m}_B. \tag{11}$$

Commonly, $\hat{n}$ is computed from the local grid. Since the boundary grid point is associated to a geometric entity through a parametric coordinate, the exact normal vector can be determined easily. Further, the pressure at the surface can be determined through a normal projection of the of the momentum equation at the wall,

$$\frac{\partial p}{\partial n} = \kappa \, \rho_B \left[\left(\vec{V}_B - \vec{g}_B \right) \cdot \hat{t} \right]^2. \tag{12}$$

Again the geometry model can be accessed to obtain the tangent vector $\hat{t}$ and the curvature of the wall κ.

TIME-DEPENDENT COMPUTATION OF THE DYNAMICS

A cell-vertex, finite-volume approximation is applied for the spatial discretization of equation 8. The discretization allows for two-dimensional and axisymmetric planar flow domains. The temporal discretization is applied using an explicit, two-stage Lax-Wendroff method [12]. The time-marching algorithm for a time step $\Delta\tau$ is of the form

$$\hat{U}_{i,j}^{*} = \hat{U}_{i,j}^{n} + \Delta\tau \, \hat{R}_{i,j}^{n}, \tag{13}$$

$$\hat{U}_{i,j}^{**} = \hat{U}_{i,j}^{*} + \Delta\tau\ \hat{R}_{i,j}^{*}, \tag{14}$$

and

$$\hat{U}_{i,j}^{n+1} = \frac{1}{2}\ \left\{\ \hat{U}_{i,j}^{n}\ +\ \hat{U}_{i,j}^{**}\ \right\}. \tag{15}$$

The $\hat{U}$ and $\hat{R}$ denote the algebraic vectors of the generalized conservative variables and flux residual, respectively. The $\hat{U}$ is defined as

$$\hat{U}\ =\ U\ V, \tag{16}$$

where V is the volume of the finite-volume cell. The $\hat{R}$ is defined as

$$\hat{R}_{i,j}\ =\ \hat{F}_{i+1/2,j} - \hat{F}_{i-1/2,j} + \hat{F}_{i,j+1/2} - \hat{F}_{i,j-1/2}, \tag{17}$$

where the flux vector for a cell face is defined as

$$\hat{F}\ =\ \mathbf{H}\cdot\hat{n}dS. \tag{18}$$

The inviscid fluxes are computed using the Roe flux-difference splitting with a TVD limiter as presented in reference [12]. The viscous fluxes are computed using differences and averages computed at the cell faces. The time step is computed using the CFL condition.

Characteristic boundary conditions are used to compute the solution points on the boundaries. The flow conditions at the compressor face boundary of the VDC inlet were applied using a variation of the method discussed in reference [13]. This involved specifying the average Mach number at the compressor face, which allowed the pressure to vary and was shown to be a non-reflecting boundary condition.

The V needed to decode $\hat{U}$ is computed from the geometric conservation law as discussed in references [14] and [15]. The geometric conservation law relates the change in volume of the cell to the motion of the cell faces and is derived from the flow integration equations with the assumption of a uniform solution for the conservative variables. The geometric conservation law follows the form of equations (13) to (15) with $\hat{U} = V$ and $\hat{R} = \hat{Z}$ where $\hat{Z}$ is the vector sum of speeds of the cell faces.

APPLICATIONS

Some preliminary inviscid computations involving dynamic grids are presented below.

Simple Hinged Flap

A simple mechanism with relative motion of its components is a plate with a hinged flap at the end of the plate. The flap is specified to rotate about its hinge in a sinusoidal manner with an amplitude of 15 degrees and a period of 0.03 seconds. The time scale of the motion is perhaps unrealistic for a flap or aileron motion on an aircraft; however, it serves to demonstrate the dynamic grid capabilities.

The analysis assumes an inviscid flow with a freestream Mach number of 2.0. The steady-state flow is obtained with the flap at zero degrees deflection and no movement of the geometry. Once the steady-state flow has been obtained, the flap is set in motion. Figure 9 shows the grid with a flap deflection of 15.0 degrees. The time-variation of the Mach number contours is shown in figure 10. The time-varying formation and disappearance of the shocks and expansions can be seen. To get some evaluation of the accuracy of the flow computation, the variation of the Mach

number at the midpoint of the upper surface of the flap during the first and third periods of the flap motion was compared to the Mach number computed from steady flow, inviscid supersonic theory [16]. Figure 11 shows that the comparison is fairly good. The computed Mach number for the compression portion of the flap motion compares well to the steady flow theory ; however, in the expansion portion, the Mach number compares less. This suggests that dynamic effects may be more significant in the expansion region.

The flap motion problem is similar to other problems of interest in aeropropulsion. One such problem is the unsteady flow about a thrust-vectored nozzle.

NASA VDC Inlet

The unsteady flow through the VDC inlet during the unstart / restart operation is now analyzed. At the cruise conditions, the inlet is in a supercritical mode in which a normal shock is positioned just aft of the centerbody bleed slot. This allows for a shorter diffuser, which saves on weight of the inlet, and for a maximum total pressure recovery. The disadvantage of this shock placement is that the shock is sensitive to flow perturbations and may unstart. During unstart, the shock moves forward in the inlet. Once past the throat, the shock is forced to be expelled from the inlet. This creates a bow shock ahead of the cowl lip, resulting in significant drag. A buzz cycle will develop if the inlet is not restarted. For the VDC inlet, restart is achieved through a slight forward translation of the centerbody, a reduction in the diameter of the centerbody, and an opening of the bypass doors to reduced the back pressure at the compressor face.

A preliminary inviscid flow computation is presented to show the nature of the flowfield during the unstart / restart operation. The steady-state flow is computed for a freestream Mach number of 2.5 with the inlet at an angle-of-attack of 0.0 degrees. The Mach number at the compressor face was set at 0.31, which is just slightly greater than the design compressor face Mach number. This places the terminal shock at a position $x/r_{cowl} = 3.25$, which is greater than the design position of $x/r_{cowl} = 2.73$.

The computed pressures along the forward portion of the centerbody compared very well with data from wind tunnel tests [7]. However, comparisons in the diffuser were not comparable since the actual flow is dominantly viscous.

The inlet is forced to unstart through an impulse at the compressor face of the Mach number of a magnitude of -0.12 over a time interval of 0.01 seconds. The pressure pulse that is created at the compressor face travels upstream in the diffuser and interacts with the terminal shock, which is then forced forward. The shock passes ahead of the throat. When the shock reaches the shock sensor, the restart process begins with a start in the motion of the centerbody. For this analysis, the centerbody was set to translate a distance of 0.2 units forward and the second cone angle rotates from an angle of 18.5 degrees to a angle of 12.5 degrees, which is equal to the angle of the nose cone. The centerbody motion occurs over a time interval of 0.05 seconds. The compressor face Mach number is increased from a value of Mach 0.31 to 0.50 to simulate the opening of the bypass doors and the reduction of the back pressure. Figure 12 shows a sequence of Mach number contours for the unstart / restart operation. The shock is expelled from the inlet and proceeds a short distance ahead of the cowl lip before returning to the cowl lip and entering the inlet. A new terminal shock begins to form in the diffuser as the flow ahead of it becomes supersonic. Once the terminal shock is formed, the centerbody returns to its design position and the compressor face Mach number returns to a value of 0.31.

The analysis of the unstart / restart flowfield continues. At this point it is evident that the motion of the centerbody is significant to the restart operation.

CONCLUSIONS

For the CFD analysis of a mechanism involving the relative motion of its components, the aspects of geometry modeling and grid generation become a function of time, as does the flow modeling, and take on an increase importance in the problem. The combined geometric approach presented in this paper has examined some of the interrelationships between the geometry modeling, grid generation, and flow modeling and has shown that these interrelationships provide for a more natural formation of the problem and can be used advantageously in the computation of the total dynamics problem.

ACKNOWLEDGEMENT

We would like to thank John D. Saunders of the NASA Lewis Research Center for providing geometry and wind tunnel test data for the VDC inlet.

REFERENCES

1. Mani, K.K. and J.W. Haney, "3D CFD Analysis of a SR71-Waverider Launch Configuration," AIAA-94-0156, January 1994.

2. Atwood, C.A., "Computation of a Controlled Store Separation from a Cavity," AIAA-94-0031, January 1994.

3. Wang, Z.J. and H.Q. Yang, "Unsteady Flow Simulation Using a Zonal Multi-Grid Approach with Moving Boundaries," AIAA-94-0057, January 1994.

4. Trépanier, J.Y., M. Reggio, M. Paraschivoiu, and R. Camarero, "Unsteady Euler Solutions for Arbitrarily Moving Bodies and Boundaries," AIAA Journal, Vol. 31, No. 10, p. 1869-1876.

5. Meakin, R.L., "Moving Body Overset Grid Methods for Complete Aircraft Tiltrotor Simulations," AIAA-93-3350, July 1993.

6. Wasserbauer, J.F., R.J. Shaw, and H.E. Neumann, "Design of a Very-Low-Bleed Mach 2.5 Mixed-Compression Inlet with 45 Percent Internal Contraction," NASA TM X-3135, 1975.

7. Saunders, J.D. and A.A. Linne, "Status of the Variable Diameter Centerbody Inlet Program," First Annual High-Speed Research Workshop. pp 1481-1504, NASA CP-10087, Part 3, April 1992. (Limited distribution).

8. Blake, M.W., P.A. Kerr, S.A. Thorp, J.J. Chou, "NASA Geometry Data Exchange Specification for Computational Fluid Dynamics (NASA IGES)," NASA RP 1338, April 1994.

9. Zeid, Ibrahim, CAD/CAM Theory and Practice, McGraw-Hill, Inc., New York, 1991.

10. Anderson, D.A., J.C. Tannehill, and R.H. Pletcher. Computational Fluid Mechanics and Heat Transfer. New York, McGraw-Hill Book Company, 1984.

11. Vinokur, M. "An Analysis of Finite-Difference and Finite-Volume Formulations of Conservation Laws." Journal of Computational Physics. 81 (1989): 1-52.

12. Liou, M.-S. and A.T. Hsu. "A Time-Accurate Finite Volume High Resolution Scheme for Three Dimensional Navier-Stokes Equations." AIAA Paper 89-1994, June 1989.

13. Chung, J., "Numerical Simulation of a Mixed-Compression Supersonic Inlet Flow," AIAA Paper 94-0583, January 1994.

14. Thomas, P.D. and C.K. Lombard. "Geometric Conservation Law and Its Application to Flow Computations on Moving Grids." AIAA Journal 17 (1979): 1030-1037.

15. Hindman, R.G. "Generalized Coordinate Forms of Governing Fluid Equations and Associated Geometrically Induced Errors." AIAA Journal 20 (1982): 1359-1367.

16. Anderson, J.D., Modern Compressible Flow. New York, McGraw-Hill Book Company, 1982.

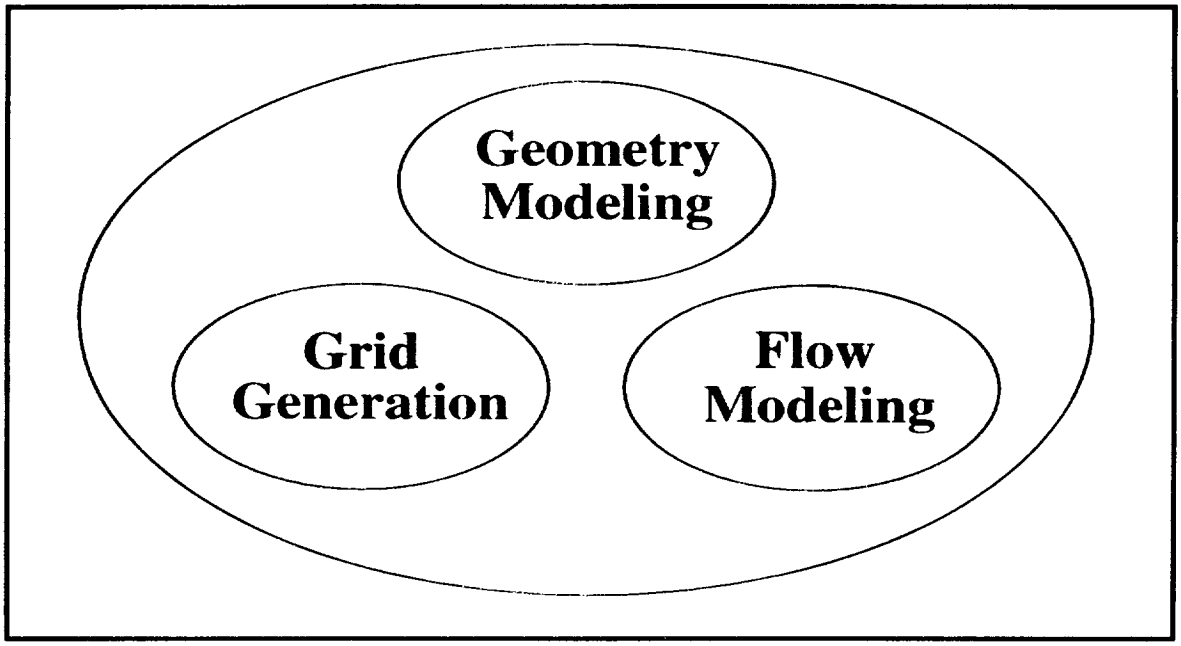

Figure 1: The aspects of the CFD analysis process: geometry modeling, grid generation, and flow modeling

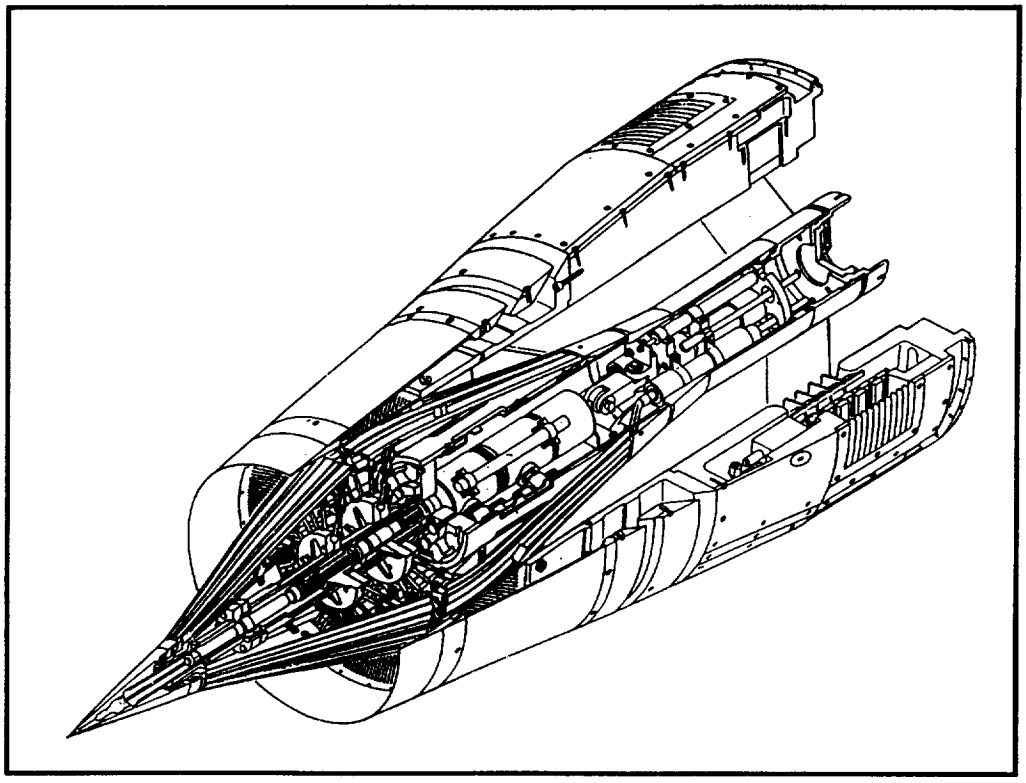

Figure 2: The mechanical design of the NASA Variable Diameter Centerbody (VDC) inlet

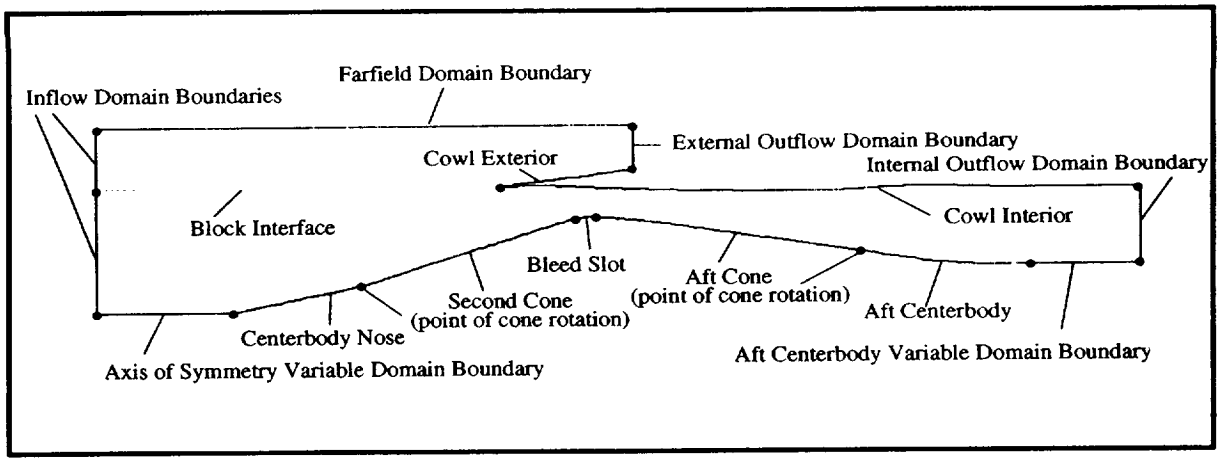

Figure 3: The entities of the planar geometry, flow domain, and block interface for the VDC inlet

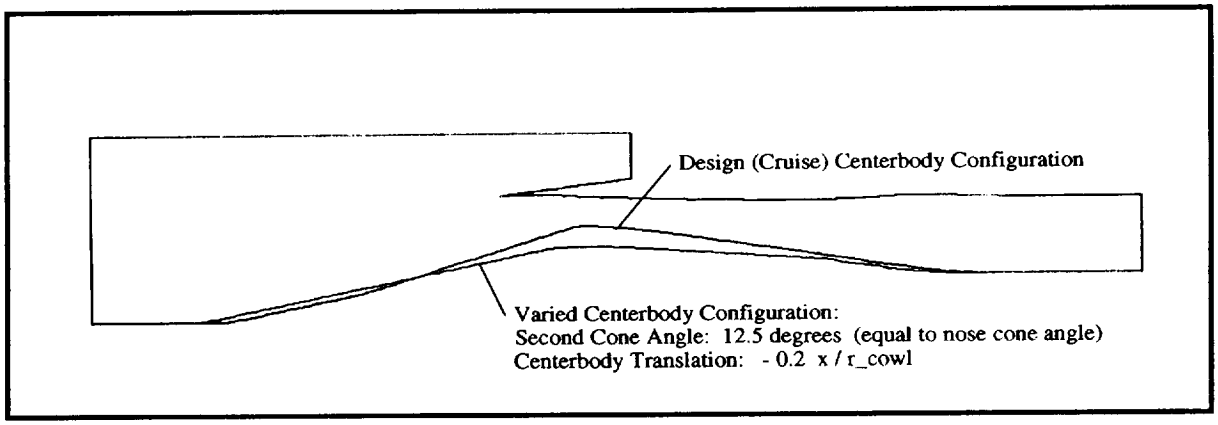

Figure 4: An example of the geometric variation of the VDC inlet

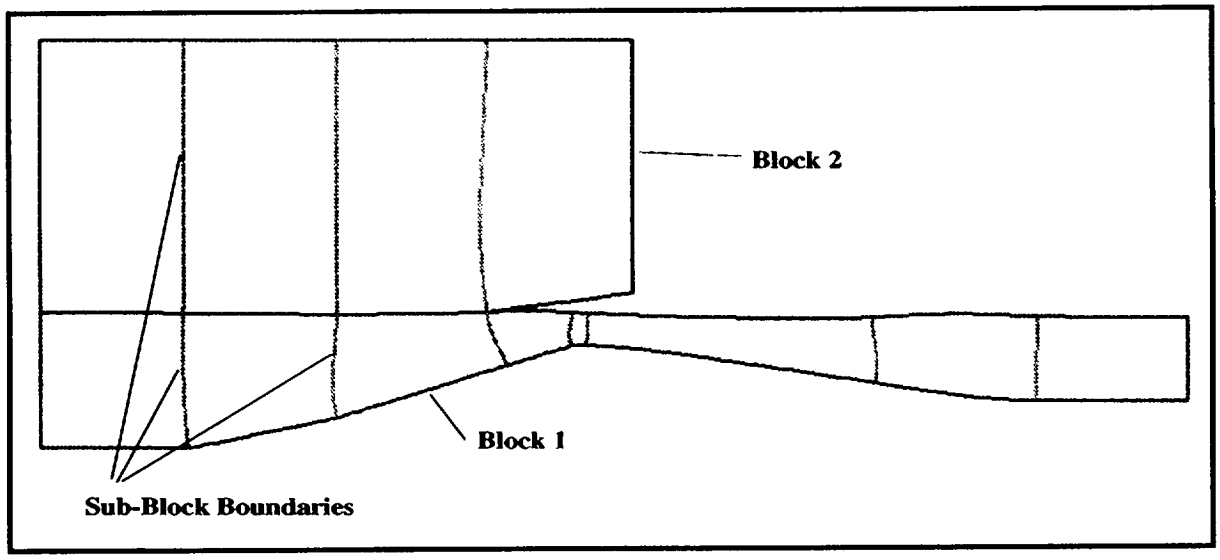

Figure 5: The block and sub-block boundaries for the grid for the VDC inlet

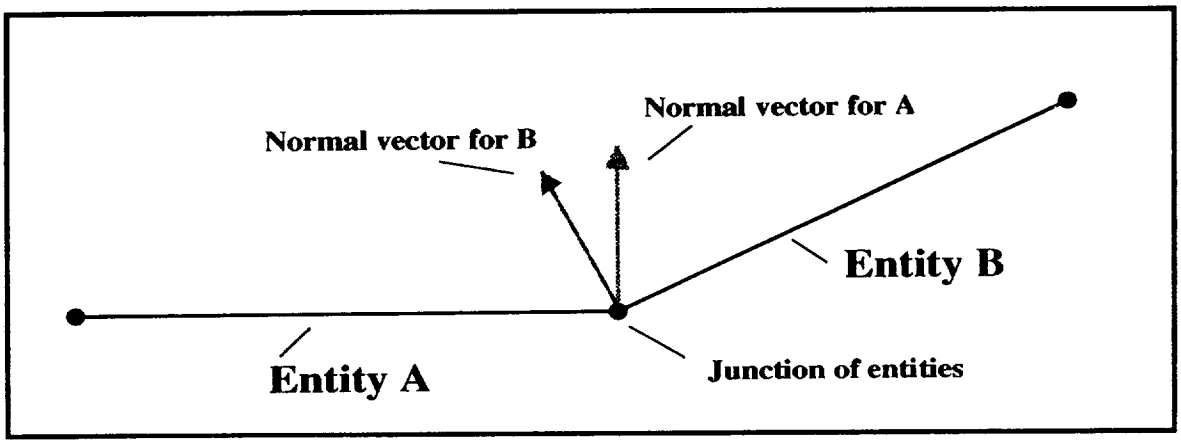

Figure 6: The junction of two entities of a planar geometry

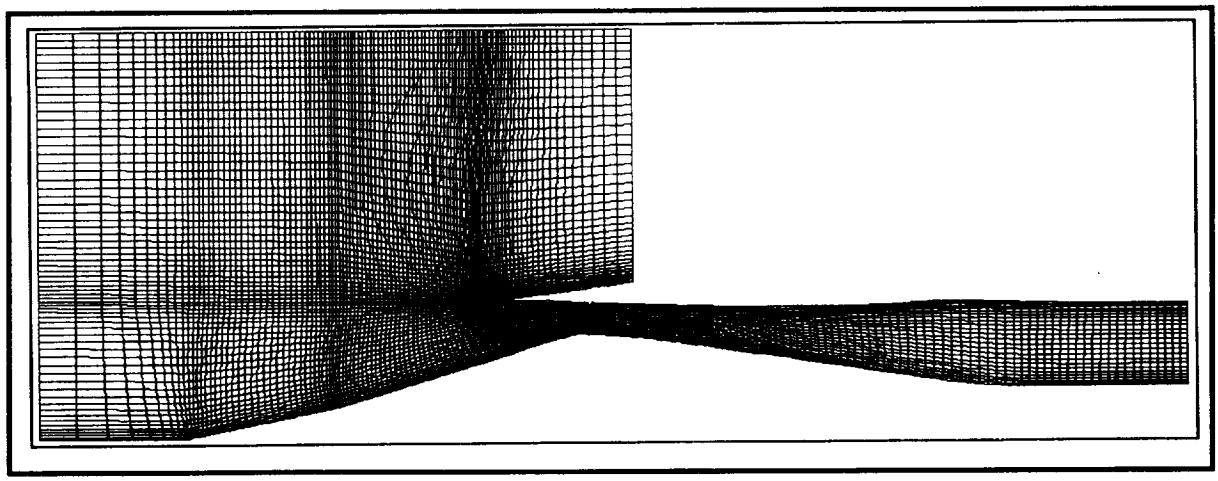

Figure 7: The multi-block grid for the inviscid analysis of the VDC inlet during the unstart / restart operation

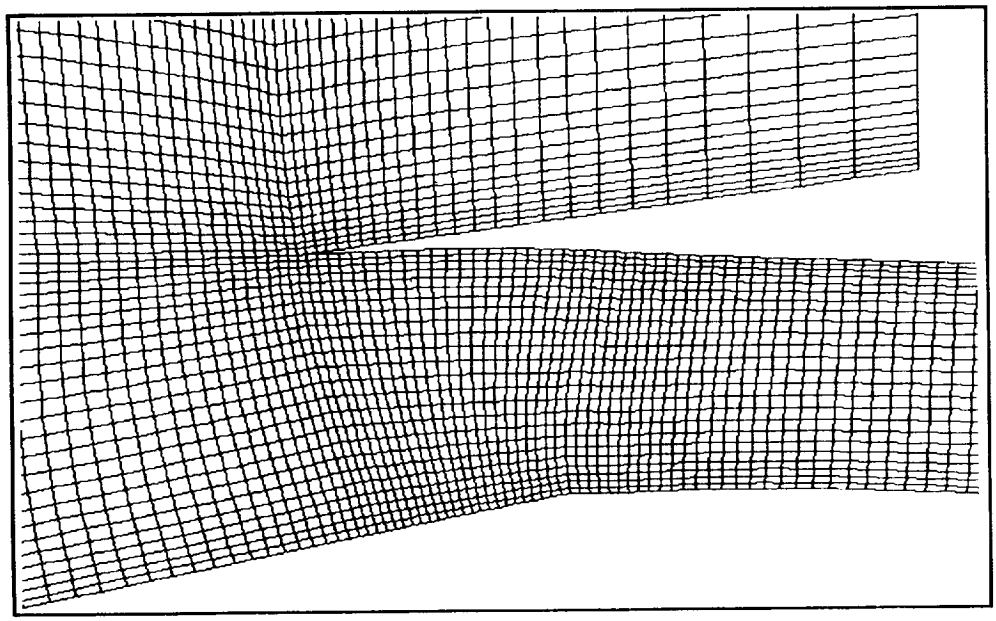

Figure 8: A closeup of the grid in the throat region of the VDC inlet with the centerbody translated and second and aft cones rotated

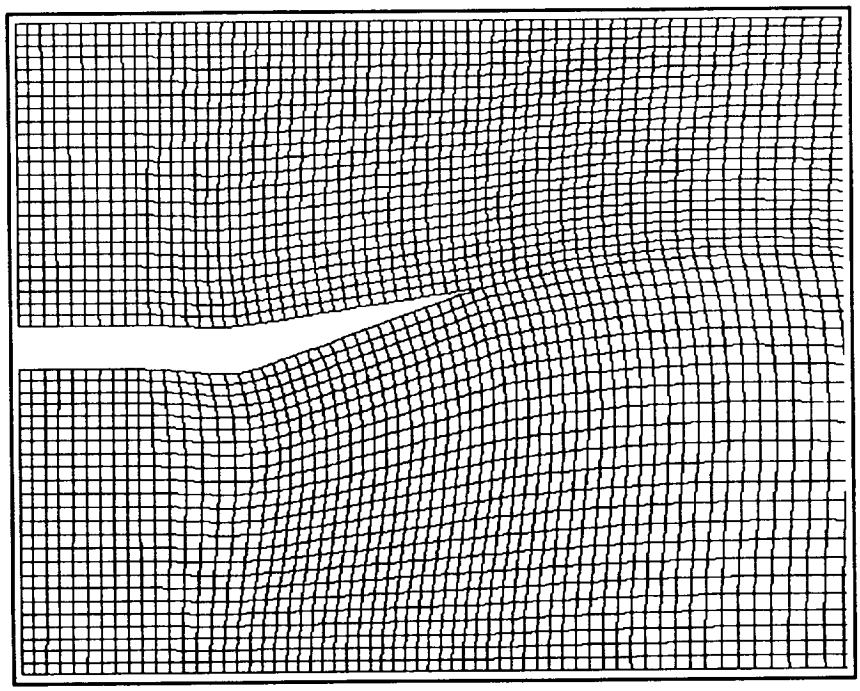

Figure 9: The grid for the hinged flap at a hinge angle of 15.0 degrees

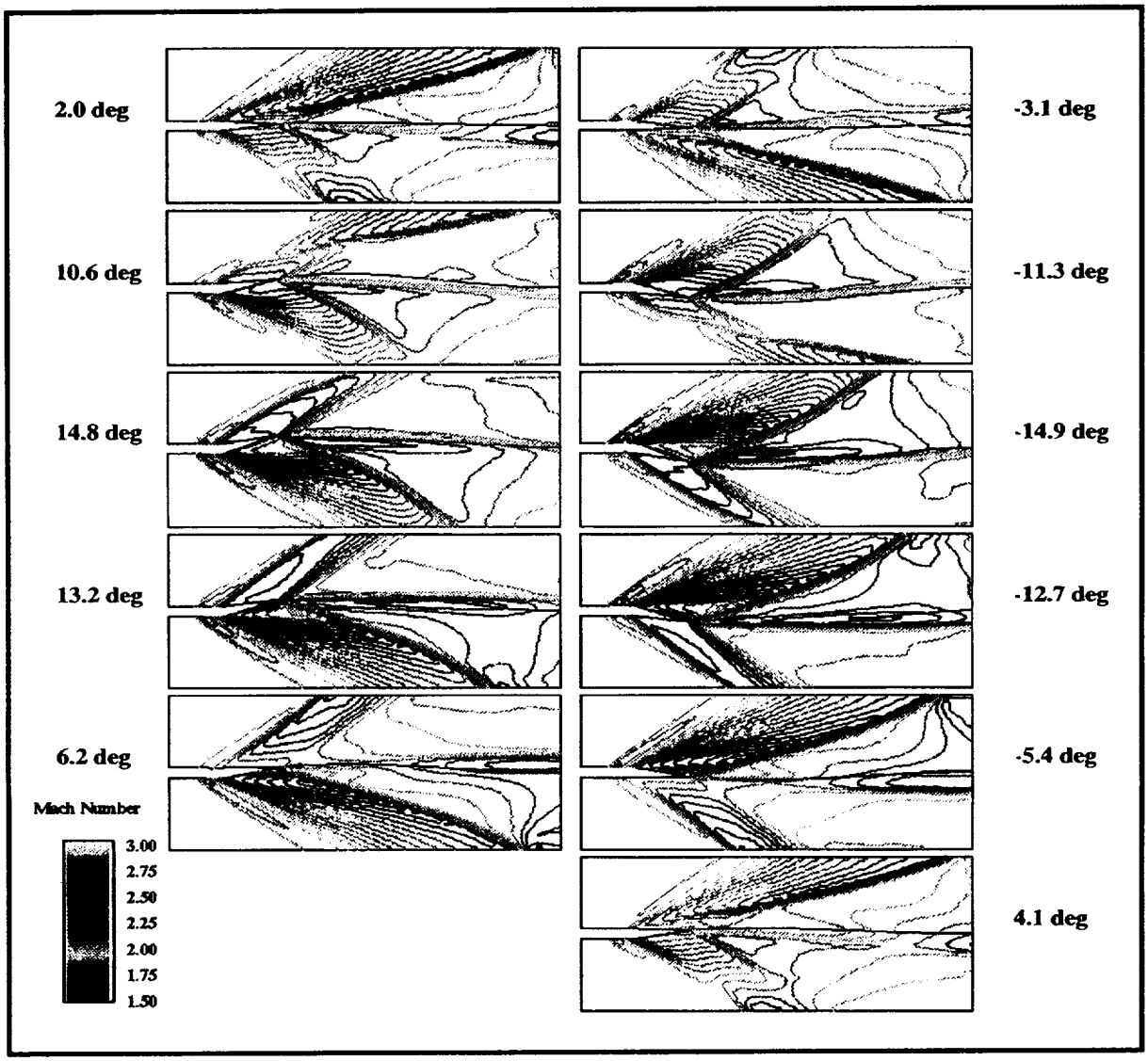

Figure 10: The sequence of Mach number contours for the inviscid analysis of the hinged flap with a freestream Mach number of 2.0 and zero degrees angle-of-attack

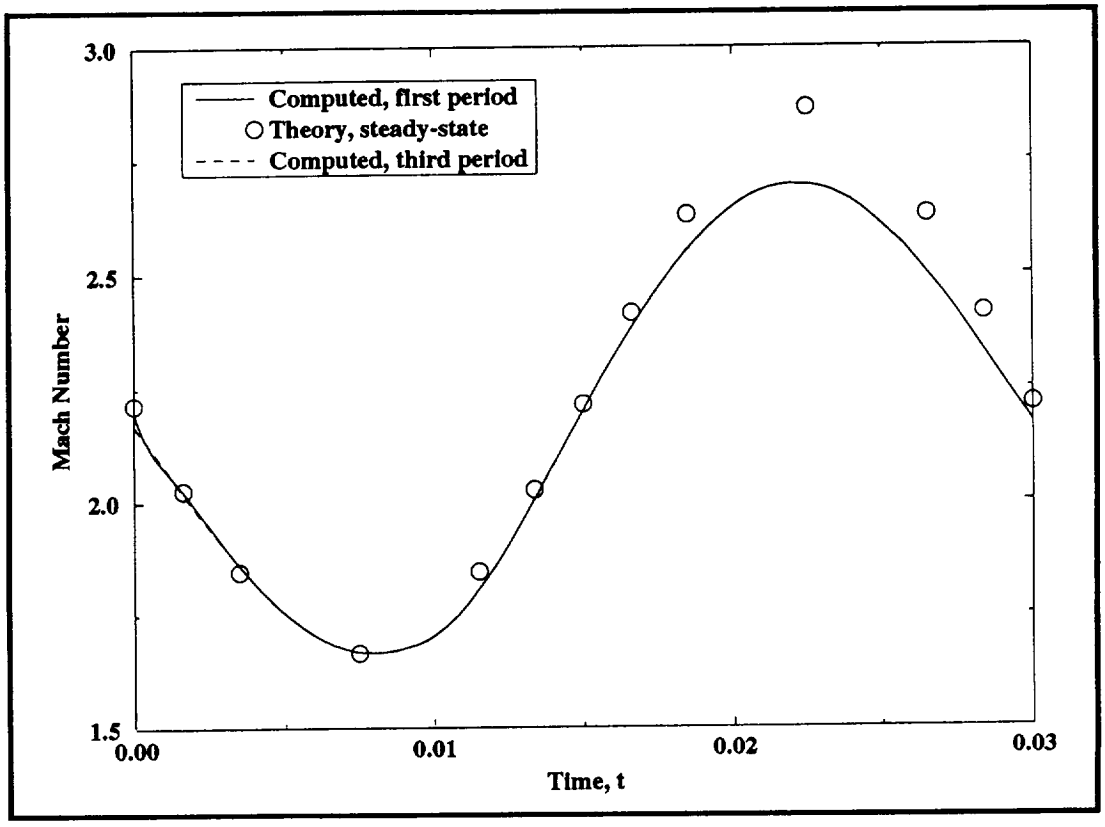

Figure 11: The comparison of the time-variation of the computed Mach numbers with the steady-state, oblique shock theory at the midpoint of the top surface of the hinged flap

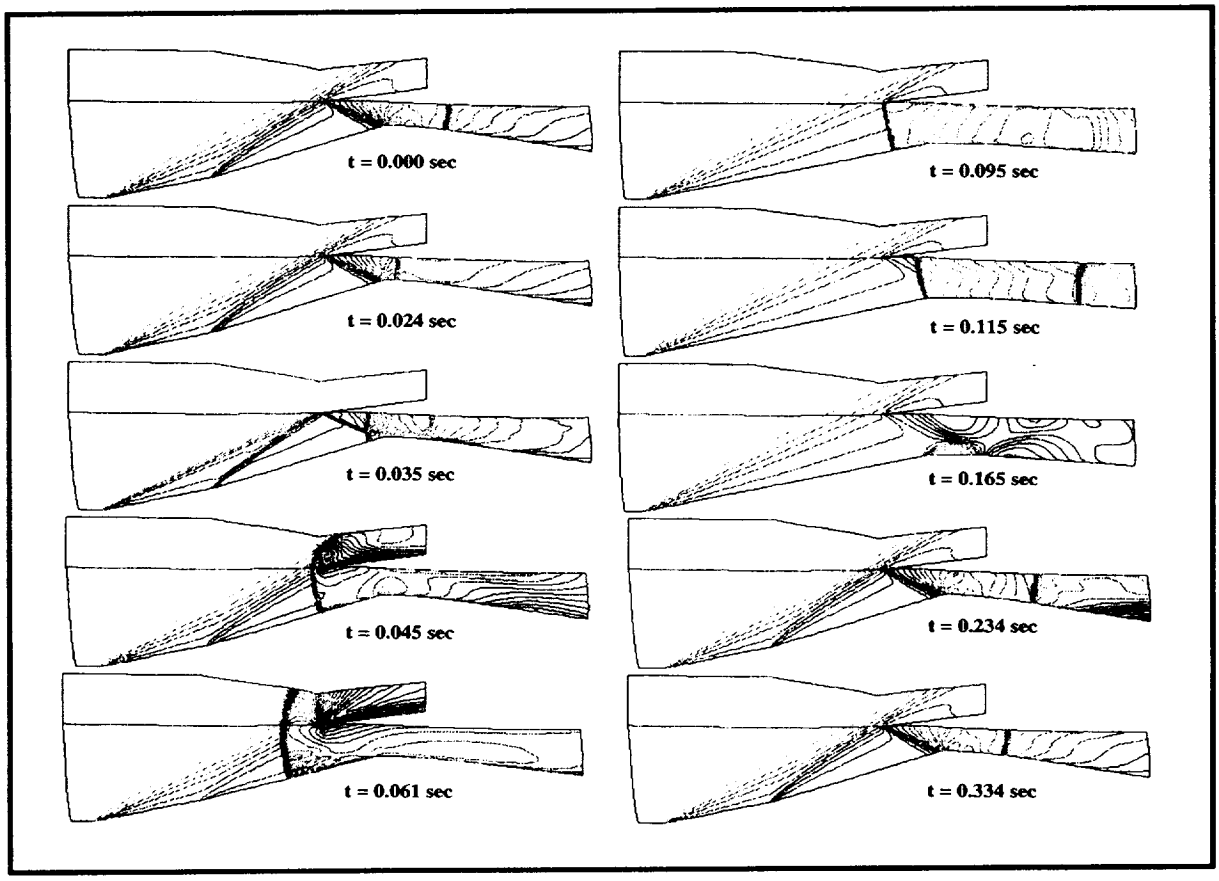

Figure 12: The sequence of Mach number contours for the inviscid analysis of the unstart / restart operation of the VDC inlet with centerbody translation and change of diameter

SOFTWARE SYSTEMS (2)